Experimental Evaluation of the Influence of Fast Movement on Virtual Antenna Arrays

Daniel Schützenhöfer*†, Erich Zöchmann*†‡, Martin Lerch†, Stefan Pratschner*†,
Herbert Groll†, Sebastian Caban†, Markus Rupp†
*Christian Doppler Laboratory for Dependable Wireless Connectivity for the Society in Motion
†Institute of Telecommunications, TU Wien, Austria
‡Department of Radio Electronics, TU Brno, Czech Republic

***Abstract*—Virtual antenna arrays are employed on the roof of high-speed trains to sound the channel between a train and a fixed base station. Because high-speed trains are moving fast during such a measurement, high Doppler shifts are experienced. In this paper, we evaluate the influence of fast movement on measurements with virtual antenna arrays if algorithms for static scenarios are employed. We have built a laboratory setup to test common algorithms such as the Bartlett beamformer. Our laboratory setup allows to compare the performance of algorithms at standstill to the performance of the same algorithms at different velocities. We show that the estimated power angular spectrum changes up to 20 dB in magnitude if we apply the same algorithm as in the static scenario. The Doppler effect also causes an angular shift. We experience that the difference in circular variance is 7.4 %. The measurement results show that DOA estimation algorithms that do not consider Doppler are not consistent anymore at fast movement.**

***Index Terms*—virtual antenna array, fast movement, angular characterisation, Doppler**

I. Introduction

Fifth generation (5G) wireless networks will not only cover stationary and low mobility users. They also support high mobility users on high-speed railways [1]. With increasing train speeds of up to $600\,\mathrm{km/h}$, there is also an increasing demand for wireless services at such velocities. To satisfy the high data rate of 5G, multiple-input multiple-output (MIMO) and massive MIMO will be used [2]. Because measurements with an antenna array on a high speed train are difficult, virtual antenna arrays are employed [3]. Virtual antenna array measurements are usually performed in stationary environments. The antenna is then only moved in between measurements [4]. The term moving virtual antenna array (MVAA) [3] describes a virtual antenna array, where the antenna is in constant motion during the measurement process. Most MVAA measurements are performed with high-speed trains. The antenna is mounted on the roof of the train. An MVAA is created by sampling data equidistantly during train movement, e.g. in [5] with a train velocity of approx. $200\,\mathrm{km/h}$. The MVAA measurements are then used for spatial characterisation [6].

The financial support by the Austrian Federal Ministry for Digital and Economic Affairs and the National Foundation for Research, Technology and Development is gratefully acknowledged. The research described in this paper was co-financed by the Czech Science Foundation, Project No. 17-18675S, and by National Sustainability Program under grant LO1401.

Our Contributions

We create a virtual antenna array and also an MVAA with the rotary unit of the TU Wien [7]–[16]. In this contribution, we firstly focus on the estimation of the angle of arrival for a stationary virtual antenna array. Then, secondly, we evaluate the impact of velocity on MVAAs. The advantage of our measurement system compared to the approach with high-speed trains is that we are capable of measuring in exactly the same environment in motion and at standstill. This allows for a fair comparison and thus for an evaluation of the Doppler impact.

II. Measurement setup

The transmit (TX) antenna is a static 7 dBi log-periodic antenna. The receive (RX) antenna is a $\lambda/4$ monopole antenna placed on a 1m long rotary arm, rotating around a central pivot. The mechanical setup of the rotary unit is shown in Fig. 1. The whole rotary unit is placed on a sliding board, that can be moved by 2λ (at 2.6 GHz) along the x-axis and by 6λ along the y-axis.

Transmit Signal

As TX signal $s(t)$, we consider an OFDM signal with a carrier frequency of approx. 2.6 GHz. We use a Zadoff-Chu sequence [17] with 72 subcarriers. With a sampling rate of 30 MSamples/s and an FFT length of 2048, we get a subcarrier spacing of approx. 15 kHz. Table I summarizes the chosen TX parameters.

TABLE I
Measurement parameters

carrier frequency	2.575 GHz
modulation type	OFDM
number of subcarriers K	72
FFT length	2048
sampling rate	30 MSamples/s
subcarrier spacing	14.648 kHz
symbol length	68.27 μs

III. Measurement without motion

In the first virtual antenna array measurement, the rotary arm is fixed to the top position. We measure uniformly a $2\,\lambda \times 6\,\lambda$ grid with a grid spacing of $0.025\,\lambda$ in both directions. The

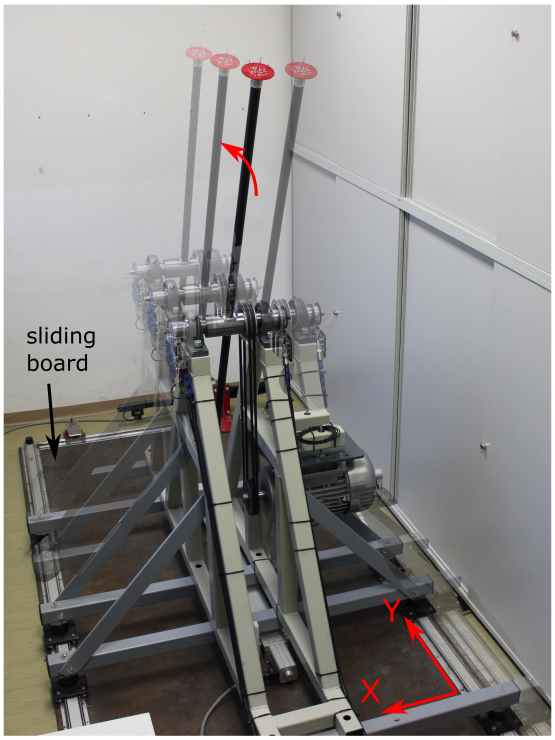

Fig. 1. Rotatory unit used to measure with the virtual antenna array and the MVAA. The whole setup can be moved in x and y direction.

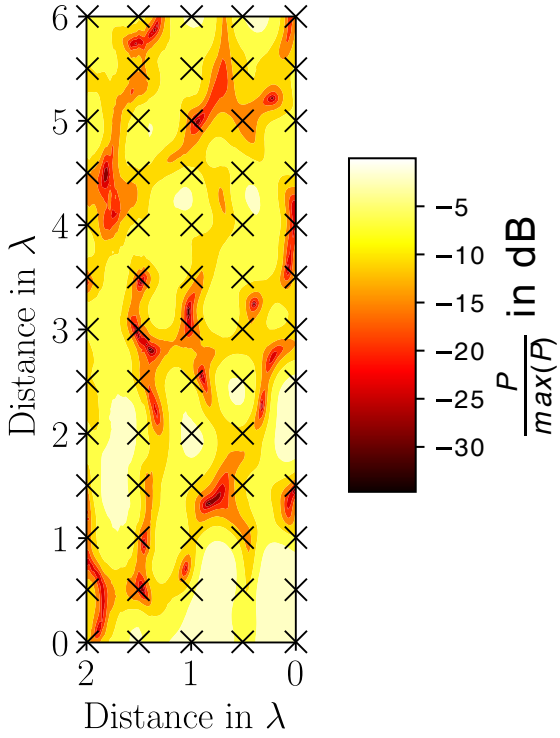

Fig. 2. Relative receive power. We experienced multipath propagation. The crosses mark the positions of the individual antenna elements for the virtual antenna measurement.

result of our measurement is shown in Fig. 2. We clearly see multipath propagation. The deepest fading holes are approx. 35 dB deep.

Direction of Arrival (DOA) Estimation

With a uniform linear array, one cannot determine the DOA unambiguously. To get a 360° coverage, we generate a uniform planar array (UPA). We take $I = 65$ sampling points with a spacing of 0.5λ in between and create an $N = 5$ times $M = 13$ UPA. The crosses in Fig. 2 mark the antenna positions. For an I-element antenna array from distinct DOAs $\theta_1 \dots \theta_\mathrm{Q}$, the output signal vector is written as

$$\underbrace{\begin{bmatrix} X_1[k] \\ X_2[k] \\ \vdots \\ X_\mathrm{I}[k] \end{bmatrix}}_{\mathbf{X}[k]} = \underbrace{\begin{bmatrix} \mathbf{a}(\theta_1) & \mathbf{a}(\theta_2) & \dots & \mathbf{a}(\theta_\mathrm{Q}) \end{bmatrix}}_{\mathbf{A}_\theta} \underbrace{\begin{bmatrix} G(\theta_1, k) \\ G(\theta_2, k) \\ \vdots \\ G(\theta_\mathrm{Q}, k) \end{bmatrix}}_{\mathbf{G}(\theta,k)} S[k] + \mathbf{N}[k]. \tag{1}$$

The vector entry $X_i[k]$ describes the noisy RX signal at the ith antenna element in the frequency domain where $k = 1 \dots K$ is the subcarrier index. The angular amplitude spectrum is represented by the vector $\boldsymbol{G}(\theta, k)$. The steering vector is denoted by $\mathbf{a}(\theta)$. The TX signal in frequency domain is expressed as $S[k]$ and $\mathbf{N}[k]$ characterize the noise vector. The steering vector $\mathbf{a}(\theta)$ of an uniform rectangular array is expressed as [18]

$$\mathbf{a}(\theta) = \mathbf{a}_\mathrm{y}(\theta) \otimes \mathbf{a}_\mathrm{x}(\theta) \tag{2}$$

where $\otimes$ denotes the Kronecker product, $\mathbf{a}_\mathrm{x}(\theta)$ is the steering vector in X direction and $\mathbf{a}_\mathrm{y}(\theta)$ is the steering vector in Y direction. The steering vectors $\mathbf{a}_\mathrm{x}(\theta)$ and $\mathbf{a}_\mathrm{y}(\theta)$ takes on the form [19]

$$\mathbf{a}_\mathrm{x}(\theta) = \begin{bmatrix} 1 & \mathrm{e}^{j\Phi_\mathrm{x}} & \dots & \mathrm{e}^{j(N-1)\Phi_\mathrm{x}} \end{bmatrix}^\mathrm{T} \tag{3}$$

$$\mathbf{a}_\mathrm{y}(\theta) = \begin{bmatrix} 1 & \mathrm{e}^{j\Phi_\mathrm{y}} & \dots & \mathrm{e}^{j(M-1)\Phi_\mathrm{y}} \end{bmatrix}^\mathrm{T} \tag{4}$$

where Φ_x and Φ_y are especially simple for a spacing of $d = \lambda/2$

$$\Phi_\mathrm{x} = -\frac{\omega}{c} d \cos(\theta) = -\pi \cos(\theta), \tag{5}$$

$$\Phi_\mathrm{y} = \frac{\omega}{c} d \sin(\theta) = \pi \sin(\theta)\ . \tag{6}$$

After back-to-back calibration of the measurement equipment and channel estimation in one step, we get

$$\hat{\mathbf{H}}[k] = \mathbf{A}_\theta \hat{\mathbf{G}}(\theta, k) = \frac{\mathbf{X}[k]}{S[k]}. \tag{7}$$

We now estimate the angular power spectrum by a conventional (or Bartlett) beamformer

$$P_\mathrm{BF}(\theta) = \frac{\mathbf{a}(\theta)^\mathrm{H} \hat{\mathbf{R}}\, \mathbf{a}(\theta)}{\mathbf{a}(\theta)^\mathrm{H} \mathbf{a}(\theta)}\ , \tag{8}$$

with the sample covariance matrix [20]

$$\hat{\mathbf{R}} = \frac{1}{K} \sum_{k=1}^{K} \hat{\mathbf{H}}[k] \hat{\mathbf{H}}[k]^\mathrm{H}\ . \tag{9}$$

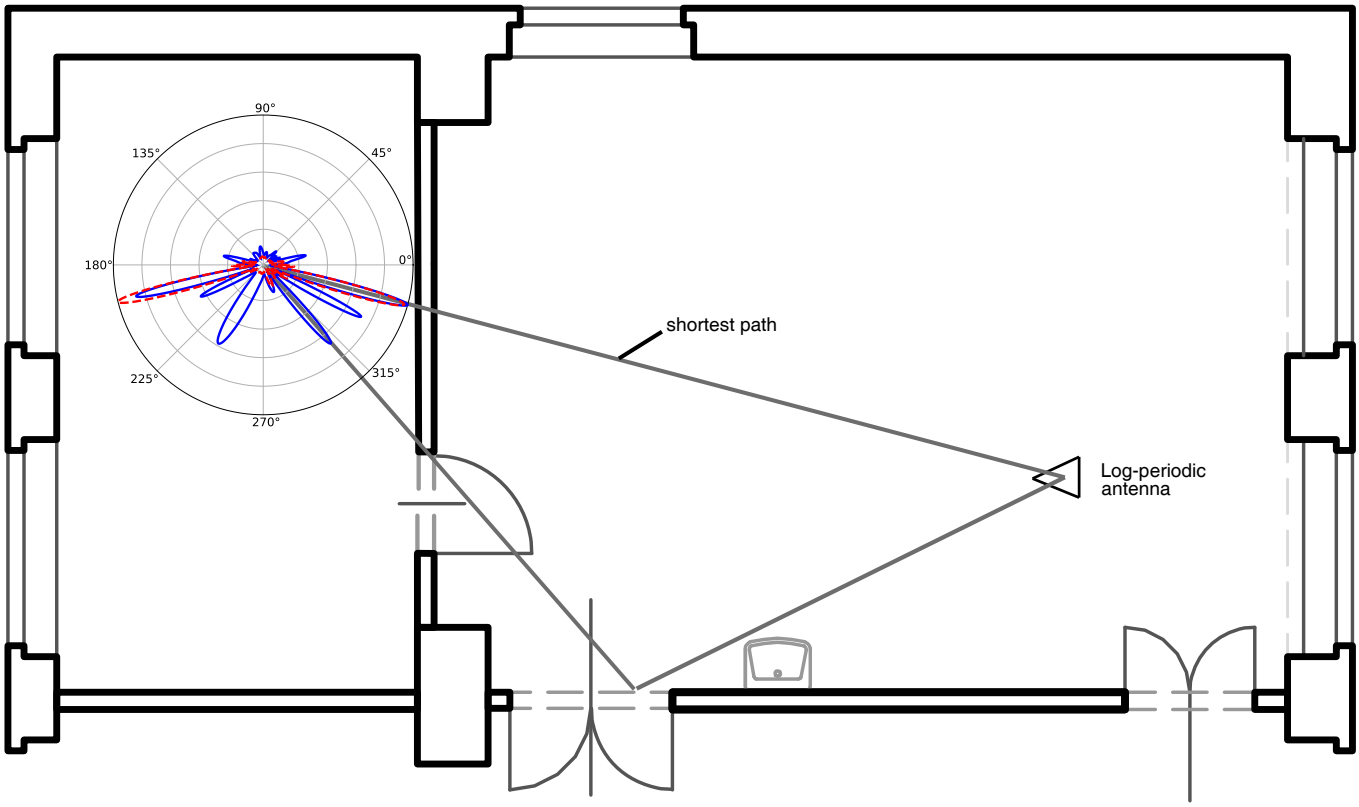

Fig. 3. Measurement environment. The blue curve shows the DOA estimated by a Bartlett beamformer at standstill. The red curve displays the DOA when the recieve antenna moves with a velocity of 200 km/h. The grey lines indecate possible multipath components.

Figure 3 shows the result of the Bartlett beamformer. Note that there are six main components. The biggest component is the direct path propagating through the wall. Two main propagation paths of propagation are marked in Fig. 3 with gray lines.

IV. Doppler Measurements

Now we are moving the RX antenna during our measurement by rotating the antenna arm. As a result, Doppler occurs. Models commonly utilized for algorithms, such as the Bartlett beamformer, MUSIC or ESPRIT, do not consider Doppler, even in the context of MVAAs [3], [5], [6], [21]. To get a first impression, we capture the Doppler spectrum at the array center position at a velocity of 90 km/h (see Fig. 4). For spectral estimation, a multitaper estimator employing discrete prolate spheroidal sequences (DPSS) is applied. The peak at $\nu/\nu_{\max} = 0$ is caused by crosstalk of the measurement equipment. Note the strong Doppler component at $\nu/\nu_{\max} = -0.5$ and a few smaller ones. The black dashed line indicates the estimated noise level.

V. Measurement in motion

Now the virtual antenna array is measured again, but this time, the receiving antenna is moving with 200 km/h. To ensure that we measure at the exact same antenna position as in the static scenario, we use a trigger signal given by a light barrier. The measurement environment, equipment, and settings remain exactly the same as in the measurement

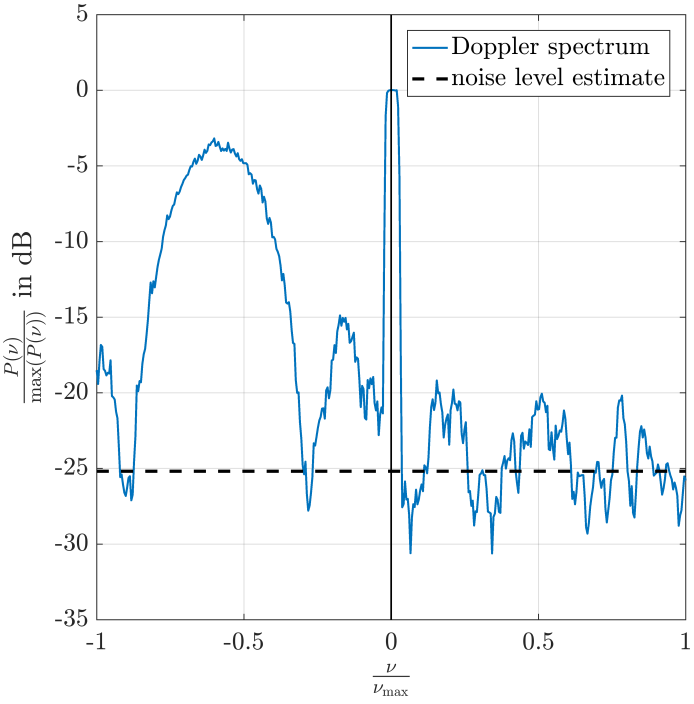

Fig. 4. Normalized Doppler spectrum. The receive antenna is moving with a velocity of 90 km/h.

without movement. The red dashed curve in Fig. 3 shows the resulting normalized angular power spectrum using the same Bartlett beamformer as at standstill. Figure 5 shows the same results on a logarithmic scale. In this figure we can better assess the difference in power. The smallest influence of the Doppler effect on the angular power is visible for the direct path component. There the magnitude differs by 1dB. The rest of the angular power spectrum completely changes. The magnitude varies up to 20 dB. Furthermore, we recognize an angular shift of the whole spectrum except the direct path component. As a result, the DOA can not be accurately determined anymore.

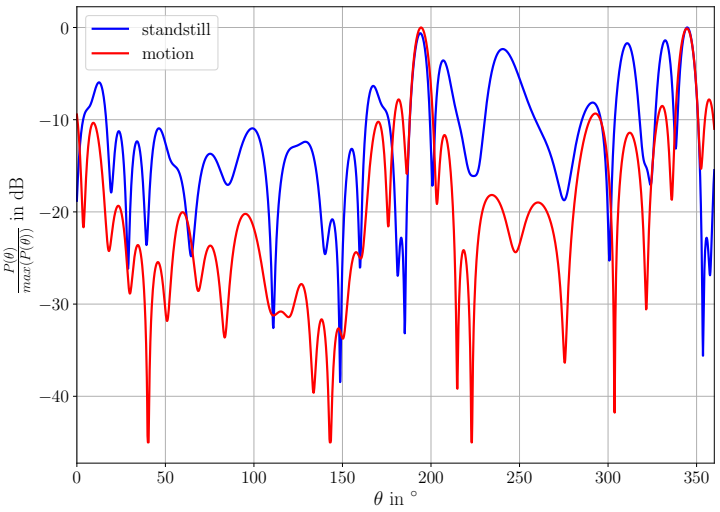

Fig. 5. The blue curve shows the angular power spectrum at standstill. The red curve displays the angular power spectrum when the recieve antenna moves with a velocity of 200 km/h.

Circular Variance and Angular Mean

The circular variance σ_θ^2 indicates the variation of the angles about the mean direction. Its possible range is between zero and one. A circular variance of one means that the DOAs are uniformly distributed between 0 and 2π. If the circular variance goes to zero, all of the DOAs are focused at one angle. The angular variance is commonly defined [22]–[24] by $\sigma_\theta^2 = 1 - |\bar{\theta}|$, where $\bar{\theta}$ is the mean direction. However, as we obtain an estimate of the directional power spectrum from (8), we use the definition of [25]. There the mean direction is defined by

$$\bar{\theta} = \int_0^{2\pi} \mathrm{e}^{j\theta} P(\theta) \mathrm{d}\theta, \tag{10}$$

where $P(\theta)$ is the direction power spectrum, calculated through

$$P(\theta) = \frac{P_{\mathrm{BF}}}{\int_0^{2\pi} P_{\mathrm{BF}}(\theta) \mathrm{d}\theta}. \tag{11}$$

The angular variance is defined by

$$\sigma_\theta^2 = \int_0^{2\pi} |\mathrm{e}^{j\theta} - \bar{\theta}| P(\theta) \mathrm{d}\theta \tag{12}$$

$$= 1 - |\bar{\theta}|^2. \tag{13}$$

This definition is comparable with the Doppler spread and delay spread. Table II shows the calculated results of the mean direction and circular variance. As mentioned before, the whole angular power spectrum is shifted if the RX antenna is in motion. This shift has an effect on the mean angle, which differs about 2.5°. We observe that the circular variance in the moving scenario is bigger than the circular variance at standstill. A smaller circular variance means that more power is centered around the mean angle. In Figure 5 we see that in the standstill scenario, more power is located at the region around 280°. If we use an algorithm for DOA estimation that does not consider the Doppler effect, the difference in circular variance is 7.4 %. This value is not negligible, we should consider other DOA estimation algorithms, that take Doppler into account.

TABLE II
COMPARISION OF THE MEASUREMENT RESULTS

	$\lvert\bar{\theta}\rvert$	$\measuredangle\,\bar{\theta}$	σ_θ^2
standstill	0.378	277°	0.8571
motion	0.281	280.5°	0.9209
difference	34.4%	1.2%	7.4%

VI. CONCLUSION

In this contribution, we introduce a laboratory setup to evaluate the influence of fast movement on virtual antenna arrays. Our measurement results show that the estimated angular power spectrum change due Doppler, if common algorithms such as the Bartlett beamformer are applied. If the RX antenna is moving with 200 km/h during the measurement, the estimated angular power spectrum changes up to 20 dB in magnitude. Additionally, the angular power spectrum has an angular shift of a few degrees. In our specific setup, the mean angle differs by 2.5°. The circular variance in the moving scenario is 7.4% larger. These results show, that DOA estimation algorithms that do not consider Doppler, e.g. the Bartlett beamformer, are not consistent anymore at fast movement.

REFERENCES

[1] P. Fan, J. Zhao, and C. I, "5G high mobility wireless communications: Challenges and solutions," *China Communications*, vol. 13, no. 2, pp. 1–13, N 2016.

[2] T. L. Marzetta, "Noncooperative cellular wireless with unlimited numbers of base station antennas," *IEEE Transactions on Wireless Communications*, vol. 9, no. 11, pp. 3590–3600, November 2010.

[3] T. Zhou, C. Tao, S. Salous, L. Liu, and Z. Tan, "Channel sounding for high-speed railway communication systems," *IEEE Communications Magazine*, vol. 53, no. 10, pp. 70–77, October 2015.

[4] A. Molisch, *Wireless Communications*. Wiley-IEEE Press, 2005.

[5] B. Chen, Z. Zhong, B. Ai, and D. G. Michelson, "Moving virtual array measurement scheme in high-speed railway," *IEEE Antennas and Wireless Propagation Letters*, vol. 15, pp. 706–709, 2016.

[6] T. Zhou, C. Tao, S. Salous, and L. Liu, "Measurements and analysis of angular characteristics and spatial correlation for high-speed railway channels," *IEEE Transactions on Intelligent Transportation Systems*, vol. 19, no. 2, pp. 357–367, Feb 2018.

[7] S. Caban, J. Rodas, and J. A. García Naya, "A methodology for repeatable, off-line, closed-loop wireless communication system measurements at very high velocities of up to 560 km/h," in *Proc. IEEE International Instrumentation and Measurement Technology Conference (I2MTC2011)*, 2011.

[8] E. Zöchmann, S. Caban, M. Lerch, and M. Rupp, "Resolving the angular profile of 60 GHz wireless channels by delay-Doppler measurements," in *IEEE Sensor Array and Multichannel Signal Processing Workshop (SAM)*. IEEE, 2016, pp. 1–5.

[9] J. Rodríguez-Piñeiro, M. Lerch, T. Domínguez-Bolaño, J. A. García-Naya, S. Caban, and L. Castedo, "Experimental assessment of 5G-candidate modulation schemes at extreme speeds," in *IEEE Sensor Array and Multichannel Signal Processing Workshop (SAM)*. IEEE, 2016, pp. 1–5.

[10] S. Caban, R. Nissel, M. Lerch, and M. Rupp, "Controlled OFDM measurements at extreme velocities," in *Proc. of 6th Extreme Conference on Communication and Computing (ExtremeCom)*. Association for Computing Machinery (ACM), USA, 2014.

[11] M. Lerch, S. Caban, E. Zöchmann, and M. Rupp, "Quantifying the repeatability of wireless channels by quantized channel state information," in *IEEE Sensor Array and Multichannel Signal Processing Workshop (SAM)*. IEEE, 2016, pp. 1–5.

[12] J. Rodríguez-Piñeiro, M. Lerch, J. A. García-Naya, S. Caban, M. Rupp, and L. Castedo, "Emulating extreme velocities of mobile LTE receivers in the downlink," *EURASIP Journal on Wireless Communications and Networking*, vol. 2015, no. 1, p. 106, 2015.

[13] M. Lerch, "Experimental comparison of fast-fading channel interpolation methods for the LTE uplink," in *57th International Symposium ELMAR*. IEEE, 2015, pp. 5–8.

[14] R. Nissel, M. Lerch, and M. Rupp, "Experimental validation of the OFDM bit error probability for a moving receive antenna," in *IEEE 80th Vehicular Technology Conference (VTC2014-Fall)*. IEEE, 2014, pp. 1–5.

[15] S. Caban, A. Disslbacher-Fink, J. A. García-Naya, and M. Rupp, "Synchronization of wireless radio testbed measurements," in *IEEE International Instrumentation and Measurement Technology Conference*. IEEE, 2011, pp. 1–4.

[16] M. Lerch, S. Caban, M. Mayer, and M. Rupp, "The Vienna MIMO testbed: Evaluation of future mobile communication techniques." *Intel Technology Journal*, vol. 18, no. 3, 2014.

[17] D. Chu, "Polyphase codes with good periodic correlation properties (corresp.)," *IEEE Transactions on Information Theory*, vol. 18, no. 4, pp. 531–532, 1972.

[18] X. He and Z. Zhang, "DOA estimation with uniform rectangular array in the presence of mutual coupling," in *2nd IEEE International Conference on Computer and Communications (ICCC)*, Oct 2016, pp. 1854–1859.

[19] S.-J. Yu and J.-H. Lee, "Design of two-dimensional rectangular array beamformers with partial adaptivity," *IEEE Transactions on Antennas and Propagation*, vol. 45, no. 1, pp. 157–167, Jan 1997.

[20] H. Krim and M. Viberg, "Two decades of array signal processing research: the parametric approach," *IEEE Signal Processing Magazine*, vol. 13, no. 4, pp. 67–94, July 1996.

[21] T. Zhou, C. Tao, L. Liu, H. Wen, and N. Zhang, "Virtual SIMO measurement-based angular characterization in high-speed railway scenarios," in *IEEE 85th Vehicular Technology Conference (VTC Spring)*, June 2017, pp. 1–5.

[22] K. V. Mardia and P. E. Jupp, *Directional Statistics*, May 2008.

[23] P. Berens *et al.*, "Circstat: a MATLAB toolbox for circular statistics," *J Stat Softw*, vol. 31, no. 10, pp. 1–21, 2009.

[24] A. Pewsey, M. Neuhäuser, and G. D. Ruxton, *Circular statistics in R*. Oxford University Press, 2013.

[25] B. H. Fleury, "First-and second-order characterization of direction dispersion and space selectivity in the radio channel," *IEEE Transactions on Information Theory*, vol. 46, no. 6, pp. 2027–2044, 2000.